Supplementary Materials for Stimulated X-ray Emission Spectroscopy in Transition Metal Complexes

Thomas Kroll[1,2],* Clemens Weninger[3,1],† Roberto Alonso-Mori[1], Dimosthenis Sokaras[2], Diling Zhu[1], Laurent Mercadier[3], Vinay P. Majety[3], Agostino Marinelli[4], Alberto Lutman[4], Marc W. Guetg[4], Franz-Josef Decker[4], Sébastien Boutet[1], Andy Aquila[1], Jason Koglin[1], Jake Koralek[1], Daniel P. DePonte[1], Jan Kern[1,5], Franklin D. Fuller[5], Ernest Pastor[5], Thomas Fransson[6], Yu Zhang[6], Junko Yano[5], Vittal K. Yachandra[5], Nina Rohringer[3,7,8],‡ and Uwe Bergmann[1,6§]

[1] *LCLS, SLAC National Accelerator Laboratory, Menlo Park, CA 94025, USA*

[2] *SSRL, SLAC National Accelerator Laboratory, Menlo Park, CA 94025, USA*

[3] *Max Planck Institute for the Structure and Dynamics of Matter, 22761 Hamburg, Germany.*

[4] *Accelerator Directorate, SLAC National Accelerator Laboratory,Menlo Park, CA 94025, USA*

[5] *Molecular Biophysics and Integrated Bioimaging Division, Lawrence, Berkeley National Laboratory, Berkeley, CA 94720, USA*

[6] *Stanford PULSE Institute, SLAC National Accelerator Laboratory, Menlo Park, CA 94025, USA*

[7] *DESY - Deutsches Elektronen Synchrotron, 22607 Hamburg, Germany. and*

[8] *University of Hamburg, 22761 Hamburg, Germany.*

Materials and Methods

The experimental setup as used at the LCLS CXI instrument (see Ref 26 in main text) is sketched in Figure 1a. The incoming X-ray pulses (10-30 fs) were tuned to 6.6 keV just above the Mn K-edge to maximize the Mn 1s absorption cross section. They were focused onto a liquid jet (200 μm at the beam interaction) with an estimated spot size of $\sim$150 nm diameter (Ref 27 in main text) and focal depth of $\sim$200 μm, resulting in a slab-like pumped medium of large aspect ratio. The pulse energy was between 0.5 and 4 mJ measured by an upstream gas detector, with approximately 20% of it reaching the sample after the transport and focusing optics. This corresponds to a maximal XFEL pump intensity at the sample of 1.5×10^{20} W/cm^2 for 30 fs pulses. $MnCl_2$ (we prepared a 5 M solution) and the $NaMnO_4$ (4 M solution) were obtained from Sigma-Aldrich and delivered into the X-ray beam with a jet using HPLC (high-performance liquid chromatography) and peristaltic pumps with a flow rate of 40 m/s. LCLS was operated at an X-ray pulse rate of 30 Hz to ensure jet stability.

The vertical divergence of the focused X-ray beam was two mrad. Si analyzers were employed in the vertical scattering geometry (see Figure 1a) dispersing the Mn Kα spectrum vertically onto a 2d detector. For spectra shown in Figures 2 and 3, $\sim$30 fs pulses and a Si(111) crystal with an intrinsic angular resolution of 49 μrad at 5.9 keV (σ polarization) were used. This corresponds to an energy resolution of 0.8 eV, and the corresponding efficiency of detecting stimulated emission with 2 mrad divergence is 2.5%. The spectra shown in Figure 4 were collected using $\sim$10 fs X-ray pulses and a Si (220) analyzer crystal with a 1 degree asymmetric cut (41 μrad angular resolution, 0.4 eV energy resolution and 2.1% detection efficiency). Images on the 2d detector were converted to emission spectra by integrating over the non-dispersive (horizontal) direction. The numbers of stimulated emission reported in the main text refer to detected photons, by integrating over the Kα_1 peak. Peak position and linewidth were determined by fitting the spectra with a Gaussian line shape.

The spontaneous XES spectra were recorded at the Stanford Synchrotron Radiation Lightsource (SSRL) at beamline 6-2 with an energy resolution of < 0.6 eV full width at half maximum (FWHM) at an incident energy of 6.6 keV).

Theoretical spontaneous XES spectra of $MnCl_2$ and $NaMnO_4$ were obtained using charge transfer multiplet calculations (see Ref 30-33 in main text). A purely ionic model was used for $MnCl_2$, with the crystal field strength 10Dq=1.0 eV being the only variable parameter.

For $NaMnO_4$, covalent mixing of ligand character is modeled using a three-configuration model including two ligand-to-metal charge transfer (LMCT) configurations (Ref 33 in main text) due to its covalent mixing (i.e. charge transfer). The used parameters were: 10 Dq = 3.0, Δ = 3.0 eV, U_{dd} = 6.0, U_{pd} = 7.0, T_{eg} = 3.5, $T_{t_{2g}}$ = 1.75. All values in eV. For simplicity, the 3d3d spin-orbit coupling as well as the 3d1s Coulomb repulsion was set to zero. All calculations were performed in O_h effective symmetry. The intensities at each transition energy (shown as sticks in Figures 3b and 4), that can also have several underlying degenerate states, were broadened with a Lorentzian of 1.6 (2.0) eV FWHM Kα_1 (Kα_2) and Gaussian with σ = 0.6 eV to account for lifetime and experimental broadening.

Theoretical results

In order to support our interpretation of the experimental results, we present here simulations of amplified spontaneous emission of a simple atomic model system of Manganese. At this stage, we do not aim for a quantitative comparison with the experiment, but want to explain the major experimentally observed trends by the simplest possible model system. We mimic the emission spectrum of the aqueous $MnCl_2$ solution by a simple few-level system of the resolved Manganese ion. We adopt an open quantum system approach as presented in Ref. 24 in the main text. The system starts out from the Mn ground state. 1s-core ionization by the XFEL populates the upper lasing state Mn $1s^{-1}$, that can decay to the lower lasing states Mn $2p^{-1}_{3/2}$ and Mn $2p^{-1}_{1/2}$ giving rise to the K α_1 and K α_2 emission, respectively. The transition-dipole moment of the K α_1 transition and the Auger-decay rate of the Mn $1s^{-1}$ and Mn $2p^{-1}$ states are chosen according to atomic Mn calculated by Krause (Ref. 42 in the main text). A sketch of the atomic level system and the corresponding radiative and Auger-decay times are presented in Figure 1.

The Liouville - von Neumann equations of the density matrix of the Mn ion are then coupled to the the one-dimensional Maxwell equation in paraxial approximation, applying the rotating wave and slowly-varying envelope approximations, as presented in Ref. 24 of the main text. For the XFEL-pump pulse, we assume a 6.6 keV photon energy and a flat-top focus profile of 200 nm radius. We assume a Gaussian temporal profile with a pulse duration of 10 fs FHWM. An adequate sampling of more realistic SASE temporal profiles would be computationally quite involving and is planned for a future project. For the sake of

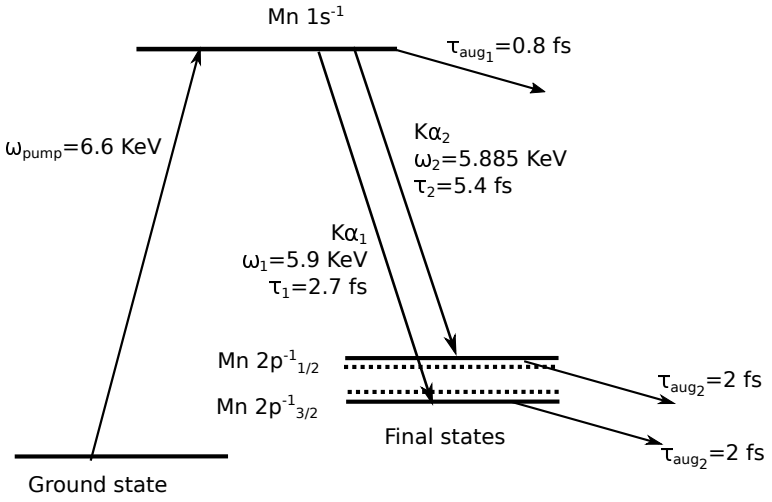

FIG. 1. The core excited state can radiatively decay to two final states separated by 15 eV that correspond to the Kα_1 ($\hbar\omega = 5.9$ keV) and Kα_2 transitions. The radiative linewidths are chosen to be 0.25 eV (≈ 2.7 fs) for the Kα_1 transition and 0.12 eV (≈ 5.4 fs) for the Kα_2 transition. The core excited and the final states can additionally decay by an Auger process and the corresponding line widths are chosen to be 0.8 eV (≈ 0.8 fs) and 0.34 eV (≈ 2 fs) respectively (the same value for both final states). Any direct coupling between the final states is neglected.

explaining the observed trends of the experimental average quantities, the results obtained using Gaussian pulses are sufficient. For a quantitative comparison and explanation of the scatter of the experimental data, a more exhaustive study simulating SASE pump pulses and more sophisticated level scheme based on charge-transfer multiplet calculations or quantum chemistry calculations for the solution is required. This is out of the scope of the current study and is planned for a future project.

Stimulated emission spectra were computed for 0.5 and 1 mJ pump-pulse energy as a function of the medium length up to 300 μm and at a density of Mn atoms of 3×10^{27} m^{-3} (corresponding to a 5 molar solution of $MnCl_2$). The pump-pulse absorption of the solvent and chlorine was taken into account (attenuation length of 111 μm). Sorting the spectra with respect to the number of photons in the emission line then allows for a qualitative comparison with the experimental spectra at similar levels of amplification (integrated gain-length product). In accordance with Figure 2 of the main paper, we plot in Figure 2 the linewidth and peak position of the $K\alpha_1$ emission, as well as the ratio of $K\alpha_2$ versus $K\alpha_1$ emission yield as a function of the number of emitted photons within the $K\alpha_1$ peak. At

an average-number of emitted photons of 10^{-2} (spontaneous emission regime), we observe emission with a the linewidth having a strict correspondence with the fluorescence of our model system. In the first two gain-lengths of the amplification regime (region A in Figure 2), the emitted spectrum shows gain narrowing and the spectral width decreases down to 0.8 eV. In the exponential gain region (region B Figure 2) which expands over several orders of ampfliciation, the emission width nearly stays constant until the onset of saturation. Beyond saturation (region C), the spectra feature saturation broadening up to about 1 eV, followed by the build-up of side peaks due to Rabi oscillations and a narrowing of the main peak. In the experiment, we only observe broadening in the saturated regime. Due to a spatial pulse profile that averages over several intensity regions, side-bands due to Rabi oscillations are not observable in the experiment.

The onset of various gain regimes, as described above in the evolution of the line width, is also reflected in the relative yield R of Kα_1 versus Kα_2 emission. In the fluorescence region, R is determined by the choice of oscillator strengths (2 in our model system). In the exponential gain regime, R grows exponentially indicating the dominant amplification of $K\alpha_1$ photons, resulting from the stronger radiative decay channel. Beyond saturation, the Kα_2 line gests amplified and the ratio decreases.

The evolution of the peak position of the Kα_1 emission line is shown in the middle panel of Figure 2: Within the numerical accuracy, the $K\alpha_1$ peak stays at the position of the the fluorescence peak throught the regions A and B. Once saturation sets in (region C), the peak shifts towards the $K\alpha_2$ transition. (Trivially, such shifts are not observed in a two-level lasing system). This indicates mixing of the final states in the strongly driven regime. That is, in the language of strong-field physics, these light-dressed states have components from both the final states. (Adding a a third level to the lower-lasing manifold in symmetric way compensates for the level shift).

In a more realistic situation, the Kα_1 and Kα_2 lines split in several multiplet components that arise from crystal field splitting. These states are closely spaced and can fall within each other's natural linewidths. We demonstrate, that this will lead to line shifts already in the exponential gain regime, as observed in the experiment. To illustrate this, we consider a 5-level system, with 2 additional radiative channels of comparable strengths and shifted by 1 eV with respect to the $K\alpha_1$ and $K\alpha_2$ transitions (the additional lines are plotted as dotted lines in Figure 1). Figure 3 presents the evolution of spectra for increasing medium

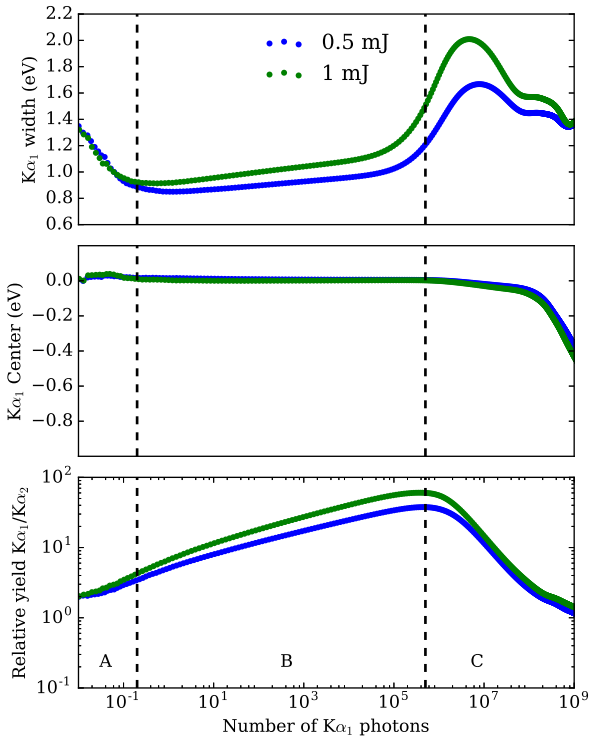

FIG. 2. Kα_1 line widths (top panel), peak positions (center panel) and the relative yields (R) into the Kα_1, Kα_2 channels (lower panel) are shown as a function of the number of emitted Kα_1 photons. The scatter plots combines data for a number of active medium lengths ranging from 0-300 μm and pumped by pulses of energy: 0.5 mJ and 1mJ. The medium length has a correspondence with the output photon number. 0 μm length implies only spontaneous emission. At the beginning, there is only fluorescence. The vertical lines approximately demarcate the 3 gain regimes. A: onset of exponential gain regime where the spectra narrow, B: exponential gain regime that exhibits nearly constant linewidth and C: the saturated regime. In the center panel, Kα_1 fluorescence peak position is chosen to be the reference position.

length (and therefore gain length) in the exponential gain regime, for a 1mJ pump-pulse. The first plot shows the spontaneous (fluorescence) spectrum, followed by the spectra at 0.3, 0.6 and 0.9 saturation lengths. Clearly, the spectra exhibit shifts even before the onset of saturation. In classical terms, it is a system of coupled, driven oscillators, that also at small driving force exhibit a shift of the resonance frequency of the unperturbed system. The qualitative model calculations provide evidence that the observed difference in chemical

shifts of $MnCl_2$ versus $MnNaO_4$ of the spontaneous spectrum collected at the synchrotron versus the spectra taken at the beginning of the exponential gain regime (Figure 4 main text) are due to amplification effects of the few-level system.

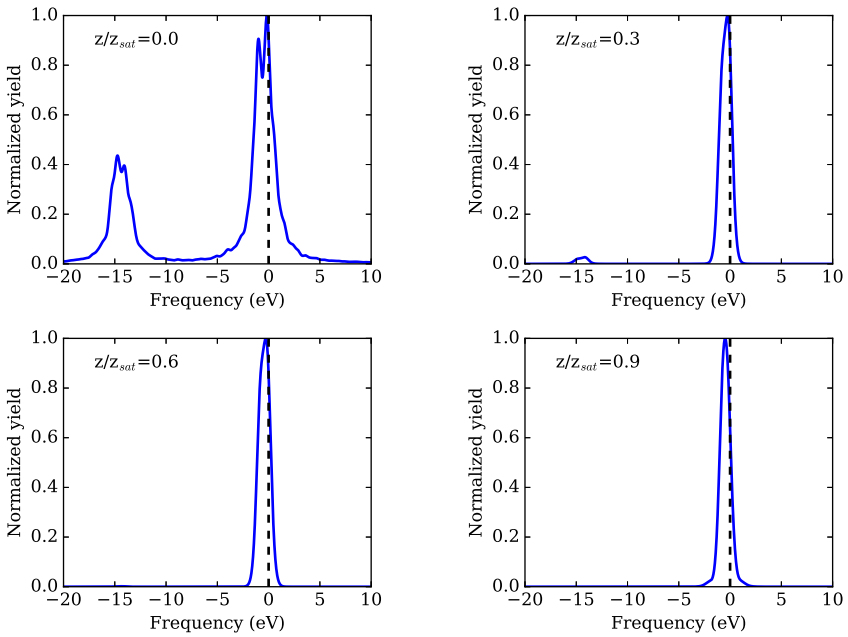

FIG. 3. Spectral evolution in the exponential gain regime with the 5-level model. The panels present spectra for increasing medium lengths (z). z_{sat} is the saturation length and $z = 0$ case shows fluorescence spectra. The peak position shifts with increasing medium lengths.

To summarize, we presented models that qualitatively explain the source of lineshifts and line broadening presented in figures 2 and 4 of the main text. To quantitatively explain the shifts between spontaneous and stimulated emission in the exponential gain regime requires a more sophisticated model that considers multiple final states within each others' linewidth. The shifts beyond saturation can be partially understood as strong-field effects in the picture of light-dressed states.

* tkroll@slac.stanford.edu

† weninc@slac.stanford.edu

‡ nina.rohringer@desy.de

§ bergmann@slac.stanford.edu